

**Chapter – 6**

*Spectroscopy of the Nucleus around Proton Shell*

*Closure Z ~ 82: Structure of  $^{195}\text{Tl}$*

### 6.1. Introduction

The thallium isotopes with proton number  $Z = 81$  is suited in a transition region between the deformed prolate rare-earth nuclei and the spherical lead nuclei at  $Z = 82$ . It is an interesting result strongly coupled band structures, which are based on  $9/2^-$  isomers, have been found in odd-mass  $^{191-201}\text{Tl}$  [1 - 6]. In the framework of the rotational model [2, 3] it has been suggested that these bands are based on the  $9/2^-$  Nilsson state originating from the  $h_{9/2}$  proton shell-model orbit. This Nilsson orbit lies close to the Fermi surface only if these odd-mass Tl nuclei have an oblate deformation [2, 3]. This is a reasonable assumption since an oblate shape has also been found for the neighbouring Hg nuclei [7, 8]. The strongly coupled bands in the odd-mass Tl nuclei show deviations from the regular rotational energy spacings. From calculations [9 - 11] in the framework of the triaxial rotor-plus-particle model the perturbation of the band structure has been attributed to an axially asymmetric shape of the Tl nuclei. In this model the nuclear shape is characterized by the deformation parameter  $\beta$  and the asymmetry parameter  $\gamma$ . The structure of these bands has been reproduced for values of  $\beta \approx 0.13$  and  $\gamma \approx 37^\circ$  indicating a predominantly oblate shape.

In the Pb and Bi isotopes the excited protons occupy the high-K  $\pi h_{9/2} i_{13/2}$  orbitals and together with the low-K  $\nu i_{13/2}^2$  neutrons form the well known shears band [12]. In heavier Hg isotopes the excited protons seem to occupy low-K  $\pi h_{11/2}^2$  orbitals and together with the low-K neutrons form highly irregular bands built of M1 and E2 transitions [13, 14]. In  $^{190}\text{Hg}$  however, a competition between these types of bands is observed [15]. The heavier Tl isotopes ( $A > 193$ ) are known only up to energy of 4 MeV and spin up to  $19\hbar$  from the studies done a long time ago [16 - 18]. None of the heavier Tl isotopes is known up to the spins where the proton pair is excited. More recent studies on these nuclei were focused on the superdeformed states [19 and references there in]. In the known deformed well the high spin states of the odd Tl nuclei are built on a high-K  $\pi h_{9/2}$  configuration. They form strongly coupled rotational bands and are associated with oblate nuclear deformation and show rotational bands built on different quasiparticle excitations [16, 18, 20 - 22].

This work presents the spectroscopic investigation of high - spin states in the  $^{195}\text{Tl}$  isotope. The phenomenon of interest in this mass region comprises of competition between prolate, oblate, triaxial shapes and competition between shears bands (involving  $\pi h_{9/2} i_{13/2}$  excitations) observed mainly in Pb, Bi and  $^{190}\text{Hg}$  isotopes and the irregular M1

bands (involving  $\pi h_{11/2}^2$  excitations) observed in the  $^{191-196}\text{Hg}$  nuclei. As stated in Chapter 1, the motivation of the present study is to observe the triaxial deformation expected for the low spin states in  $^{195}\text{Tl}$  persists at higher angular momenta and how it influences the multi-quasiparticle excitations and alignments in these nuclei. Furthermore we can study how the shears bands and the irregular  $\pi h_{11/2}$  bands compete in the Tl isotopes. We also wish to establish if the known superdeformed bands can be observed in these reactions. It should be noted that none of the heavier Tl has been studied at sufficiently high angular momenta to allow proton excitations to be observed. Thus, studying the level scheme of  $^{195}\text{Tl}$  will provide insight on the proton excitations in these nuclei and the competition between the shears bands and the irregular  $\pi h_{11/2}^2$  bands.

Many rareearth nuclei have been extensively investigated up to high spins by means of the (HI, Xn) reactions. However, only states lying on or close to the yrast line can be observed in such reactions and no information about non-yrast low spin states can be observed. A description of the high-spin phenomenon in  $^{195}\text{Tl}$  is presented in this chapter.

## 6.2. Literature Survey

The nuclear structure of light Tl nuclei is not well studied in recent times. Spectroscopy of these nuclei was done in the early 70's and most of the studies on Tl nuclei in the recent times are focused on the superdeformed states [19 and references there in]. A brief discussion of the work done earlier is presented here.

In the light odd-mass thallium nuclei, Diamond and Stephens [1] identified low-lying  $9/2^-$  isomeric state having excitation energies varying systematically with mass number. The isomeric state has a life time of 3.6 secs in  $^{195}\text{Tl}$ . In the article by Newton *et al.*, [2] the authors have studied the rotational bands in the odd-mass Tl nuclei  $^{191-197}\text{Tl}$  through (HI, xn) reactions. They have used the reactions  $^{186}\text{W}(^{14}\text{N}, 5n\gamma)^{195}\text{Tl}$  at 85, 93 MeV,  $^{197}\text{Au}(\alpha, 6n\gamma)^{195}\text{Tl}$  at 68, 74 and 80 MeV and  $^{188}\text{Os}(^{11}\text{B}, 4n\gamma)^{195}\text{Tl}$  at 57 MeV. The results of the  $\gamma$ - $\gamma$  coincidence measurements were taken with two Ge(Li) detectors. Newton *et al.*, [2] reported an inbeam study of  $^{199}\text{Tl}$ . They have found the systematic occurrence of  $11/2^-$ ,  $13/2^-$  and  $15/2^-$  states above the  $9/2^-$  isomers. They interpreted that these states formed a rotational band based on the  $K = 9/2^-$  state arising from the  $h_{9/2}$  orbital. These authors have established the level scheme of  $^{195}\text{Tl}$  upto  $\sim 1.6$  MeV in excitation energy and a spin-parity of  $15/2^-$ .

Leider et al., in 1979 [17] have populated high-spin states in  $^{195,197}\text{Tl}$  using the  $(\alpha, xn)$  reactions and studied by means of in-beam  $\gamma$ -ray and electron - spectroscopic methods. They have observed several new features in these nuclei. The  $9/2^-$  bands of  $^{195,197}\text{Tl}$  are extended to  $27/2^{(-)}$  and  $29/2^{(-)}$  respectively. These nuclei have shown a quenching of energy spacings between the  $23/2^-$ ,  $25/2^-$ ,  $27/2^{(-)}$  and  $29/2^{(-)}$  states. They have interpreted this as arising from the coupling of a  $h_{9/2}$  proton to the  $\pi h_{11/2}^{-2}$  configurations in the core nuclei  $^{194,196}\text{Hg}$ . Furthermore they have observed positive parity bands based on  $15/2^+$  states and were established up to  $35/2^{(+)}$  and  $29/2^{(+)}$  in  $^{195,197}\text{Tl}$  respectively. These bands may originate from the coupling of an  $h_{9/2}$  proton to a broken pair of neutrons. This pair consists of a rotation-aligned  $i_{13/2}$  neutron and a low-j neutron in the  $p_{1/2}$ ,  $p_{3/2}$  or  $f_{5/2}$  shell. The same is known to constitute the five bands in  $^{194,196}\text{Hg}$ .

### 6.3. Experimental Details

The  $^{195}\text{Tl}$  were populated *via* the complete fusion reaction  $^{181}\text{Ta}(^{18}\text{O}, 4n)^{195}\text{Tl}$  at beam energy of 83 MeV. The  $^{18}\text{O}$  pulsed beam (74 nsec) with a  $4^+$  charge state was delivered through the K200 Separate Sector Cyclotron facility at iThemba LABS, Cape Town, South Africa. The  $\gamma$ -rays were detected using the AFRODITE gamma array (AFRICan Omnipurpose Detector for Innovative Techniques and Experiments). The target consisted of two metal foils of  $500 \mu\text{g}/\text{cm}^2$  each. The AFRODITE detector system then consisted of 8 Compton-suppressed Clover Detectors and 6 LEPS (Low Energy Photon Spectrometers) detectors. These detectors were placed at  $45^\circ$ ,  $90^\circ$  and  $135^\circ$  respectively. Refer to chapter 3 for the figure of the AFRODITE (Fig. 3.17) array and a schematic view (Fig. 3.18) of the three detector rings. The master trigger was generated by a coincidence condition in which two or more Clover detectors has fired. In all about  $10^9$  two or higher fold events were accumulated in the list mode data during the experiment.

A systematic procedure has been adopted for the offline analysis of the list mode data obtained during the experiment. The details of the analysis procedures were explained in chapter 3. The analysis of the data is mostly done using the RADWARE [23] analysis package.



#### 6.4. Results and Discussion

The main objective of this work was to extend the level scheme of  $^{195}\text{Tl}$  to higher spins. Previously the level scheme was established up to excitation energy of  $\sim 4.5$  MeV and  $37/2^+$  in spin and parity. In the present investigation the level scheme is studied up to excitation energy of  $\sim 6$  MeV and a tentative spin-parity of  $45/2^-$  with the addition of more than 40 new  $\gamma$  transitions. These newly found transitions are placed in the level scheme with the help of  $\gamma$ - $\gamma$  coincidence measurements. The level scheme of  $^{195}\text{Tl}$  resulting from the present investigation is shown in Fig. 6.1. The  $9/2^-$  band previously known upto  $27/2^{(-)}$  (ref. [17]) has been extended to the  $45/2^{(-)}$  state. Furthermore the side band built of the  $15/2^+$  state which is previously known upto  $35/2^{(+)}$  is extended to  $45/2^{(+)}$ . Two more sidebands were found in the present analysis. They are placed on above the  $29/2^-$  level and the other above the  $33/2^+$  level (ref Fig. 6.1.). A representative  $\gamma$ - $\gamma$  coincidence spectra of various gated transitions with their respective coincidence gamma rays marked are shown in Fig. 6.2. - Fig. 6.7.

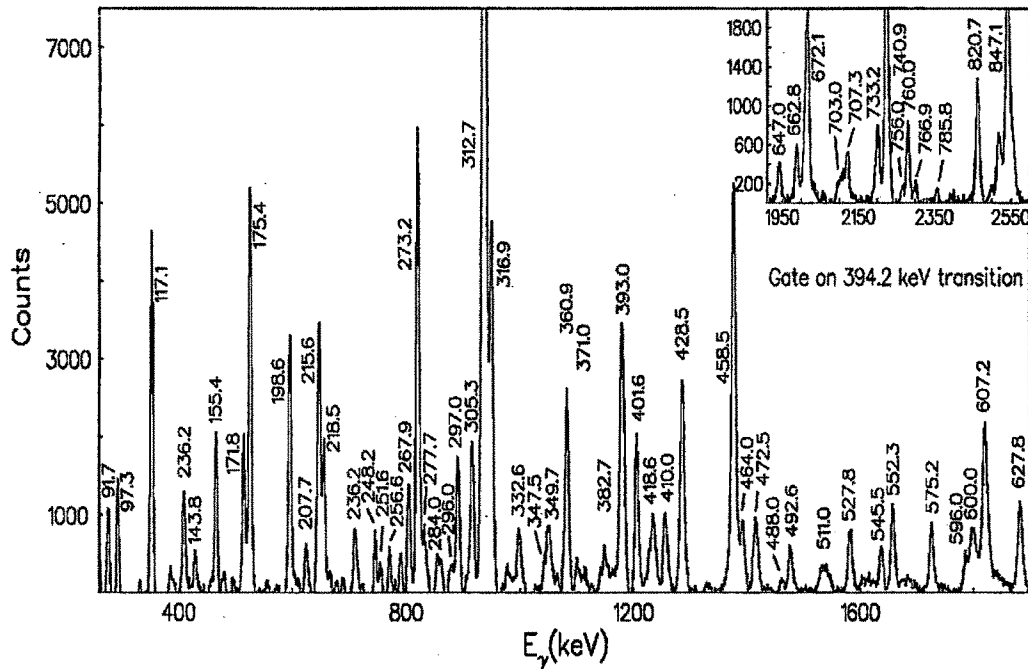


Figure 6.2:  $\gamma$ - $\gamma$  Coincidence spectrum for  $^{195}\text{Tl}$  with gate on the 394.2-keV ( $11/2^- \rightarrow 9/2^-$ ) transition. The energies are marked within  $\pm 1$  keV.

The use of Clover detector arrays and sufficient coincidence events enabled us to perform DCO (Directional Correlation from Oriented nuclei) and IPDCO (Integrated polarizational Directional Correlation from Oriented nuclei) calculations for the observed transitions. We have seen from Chapter 3 that the AFRODITE array consists of rings of Clover detectors at different angles. As described in Refs, [24 - 26], a  $\gamma$ - $\gamma$  matrix was constructed with one axis corresponding to  $\gamma$ -rays recorded by the 45° detector and the other axis corresponding to the  $\gamma$ -rays recorded by 90° detector. A gate corresponding to a  $\gamma$ -ray of known multipolarity is taken for the detector on say, the  $x$ -axis and the coincidence spectrum is projected along the other axis. Next, the same gate is set on the  $y$ -axis and the spectrum along the  $x$  axis is projected. The  $R_{DCO}$  is then defined as;

$$R_{DCO} = \frac{I_{\gamma_1 \text{ at } 90^\circ, \text{ gated with } \gamma_2 \text{ at } 45^\circ}}{I_{\gamma_2 \text{ at } 45^\circ, \text{ gated with } \gamma_1 \text{ at } 90^\circ}}$$

The resultant values of  $R_{DCO}$  for the observed transitions are illustrated in Fig. 6.8. wherein the results are obtained with the gates on known dipole transitions. The present statistics allowed us to obtain only qualitative information regarding the multiplicities of the transitions. Quantitative estimates such as mixing ratios could not be obtained due to the limited statistics in the angle dependent data analysis.

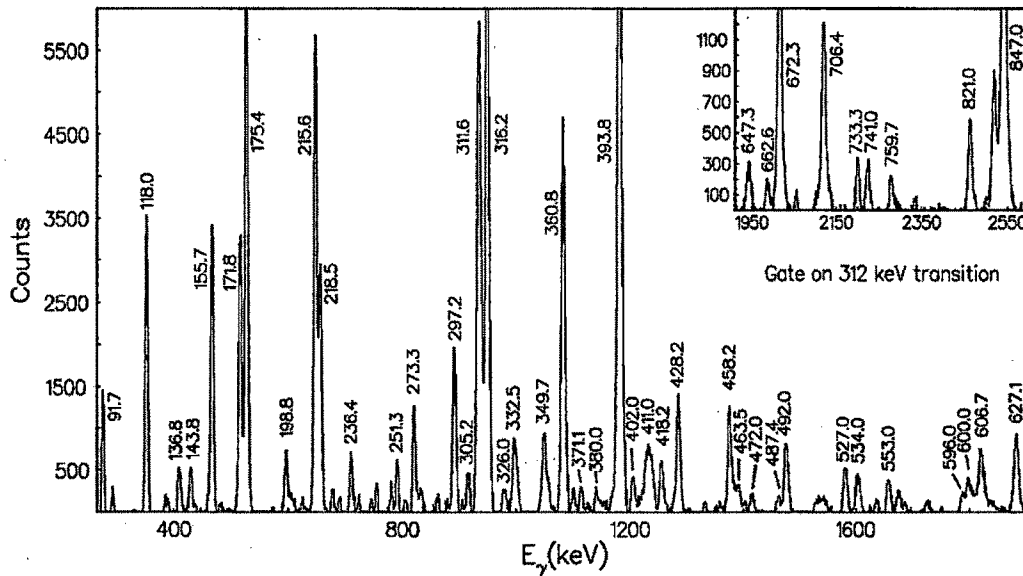


Figure 6.3:  $\gamma$ - $\gamma$  Coincidence spectrum for <sup>195</sup>Tl with gate on the 312.0-keV ( $25/2^+ \rightarrow 23/2^+$ ) transition. The energies are marked within  $\pm 1$  keV.

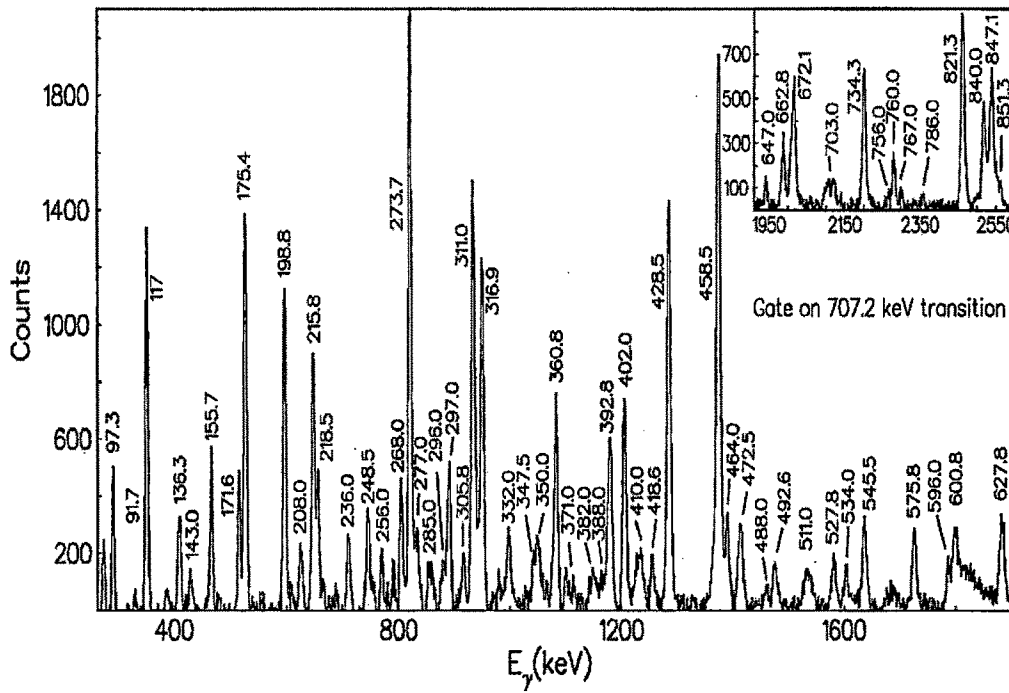


Figure 6.4:  $\gamma$ - $\gamma$  Coincidence spectrum for <sup>195</sup>Tl with gate on the 707.2-keV ( $13/2^- \rightarrow 9/2^-$ ) transition. The energies are marked within  $\pm 1$  keV.

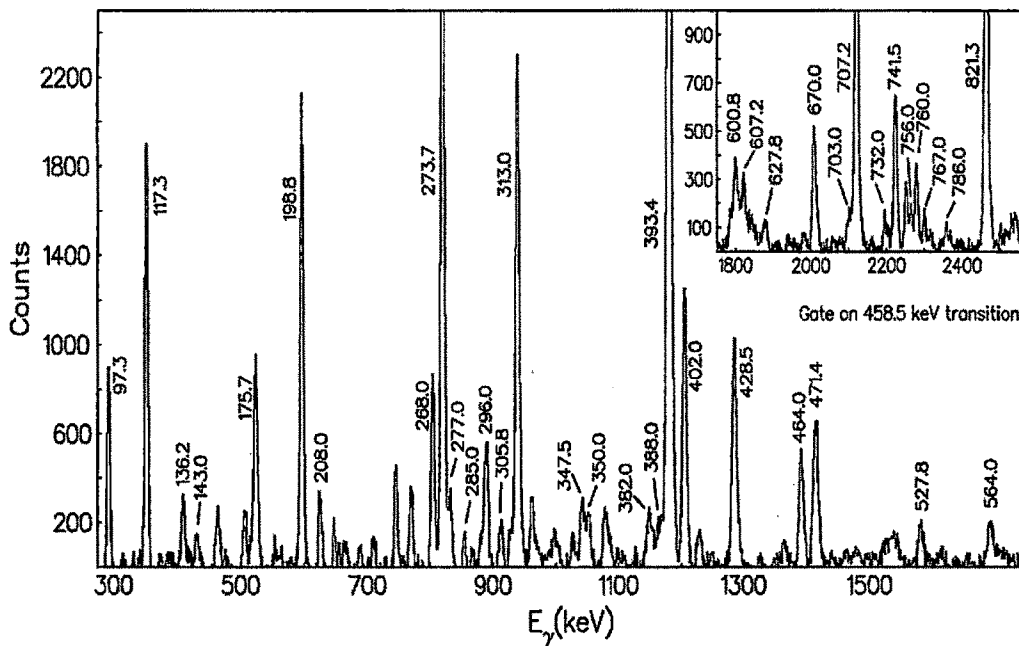


Figure 6.5:  $\gamma$ - $\gamma$  Coincidence spectrum for <sup>195</sup>Tl with gate on the 458.5-keV ( $19/2^- \rightarrow 17/2^-$ ) transition. The energies are marked within  $\pm 1$  keV.

The use of Clover detectors facilitates polarization measurements which are crucial to determine the parity of the state involved with de-excitation of the transition studied. In a Clover each of the individual crystal acts as a scatterer, while the two adjacent crystals as the absorbers. Use of an array comprised of composite detectors such as Clovers facilitates coincidence polarization measurements [27 - 29].

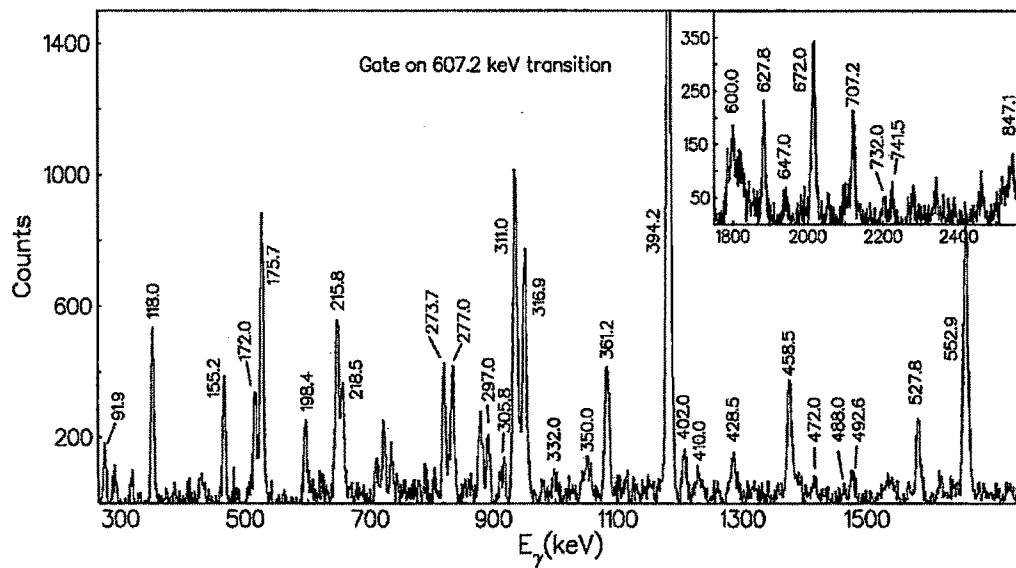


Figure 6.6:  $\gamma$ - $\gamma$  Coincidence spectrum for  $^{195}\text{Tl}$  with gate on the 607.2-keV ( $13/2^- \rightarrow 11/2^-$ ) transition. The energies are marked within  $\pm 1$  keV.

This method has unique advantage of reducing the contamination from neighbouring nuclei and background, thereby helping in a more precise assignment of the parity for the excited state whose spin value is already known. Following the procedure by Duchene *et al.* [27], the sensitivity of the Clover detector to the linear polarization of  $\gamma$ -rays is illustrated in Fig. 6.9. The anisotropy between the number of Compton scattered  $\gamma$ -rays in the reaction plane  $N_{\parallel}$ , and perpendicular to it,  $N_{\perp}$ , is indicative of the electromagnetic nature of the transition. A polarization matrix was constructed where the energy recorded in a detector was placed on one axis, while the other axis correspond to the energy scattered in a perpendicular or a parallel segment of the Clover with respect to the beam axis [30, 31]. A pure electric transition due to its preferential scattering in the perpendicular direction with respect to the beam axis results in a positive value for  $\Delta_{IPDC0}$ , while a pure magnetic transition results in a negative value for  $\Delta_{IPDC0}$  due to its

preferential scattering along the parallel direction. A near-zero value for  $\Delta_{IPDCO}$  is indicative of an admixture. Fig. 6.7 illustrates the value of asymmetry parameter for some of the observed transitions in  $^{195}\text{Tl}$ .

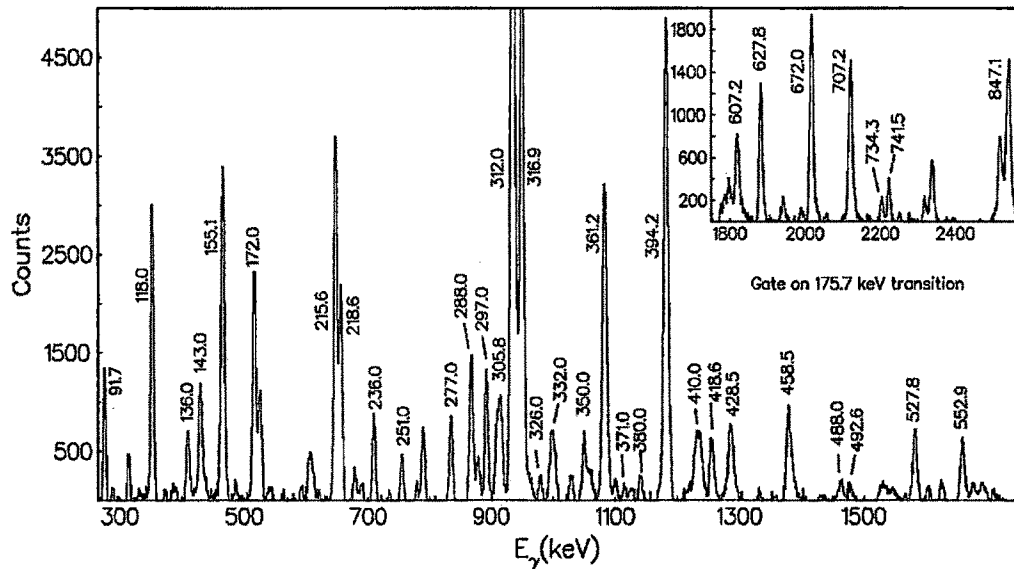


Figure 6.7:  $\gamma$ - $\gamma$  Coincidence spectrum for  $^{195}\text{Tl}$  with gate on the 175.7-keV ( $17/2^+ \rightarrow 15/2^+$ ) transition. The energies are marked within  $\pm 1$  keV.

The lowest  $\gamma$ - $\gamma$  coincidence spectrum gated is 394.2-keV (Fig. 6.2.) transition. But it has a close lying  $\gamma$ -ray 392.8-keV ( $17/2^-$ ), which may not provide a clear picture. Another striking feature in the gated spectra, is the large intensity of  $\approx 312$ -keV, which is a multiplet. When gated on the transition 312.0-keV (Fig. 6.3.) we can clearly see a strong 311.6-keV transition. A careful analysis of this multiplet yielded that this line is a triplet. So, the spectra displayed in the Fig. 6.4 - 6.7. are relatively clean spectra and from them one could clearly observe all the  $\gamma$ -transitions in coincidence. In the  $\gamma$ - $\gamma$  coincidence spectrum (Fig. 6.5.) gated on the 458.5-keV member of the  $9/2^-$  band, most probably only one component of this multiplet recurs as has been concluded from the reduced intensity of this line. The multipolarity measurements for this transition are 0.91 (0.13) and -0.08 (0.02) for DCO and IPDCO respectively. These indicate that this transition is a magnetic dipole transition. Hence this component of 313.0-keV has been assigned  $13/2^- \rightarrow 11/2^-$  member of the  $9/2^-$  band. In the other coincidence spectrum (Fig. 6.7.) gated on the 175.7-keV member of the side band, the 312-keV multiplet is again the strongest peak in the

spectrum. The 175.7-keV appears to be in coincidence with all three components of the  $\approx 312$ -keV multiplet. A careful determination of coincidence intensities for all relevant  $\gamma$ - $\gamma$  coincidence spectra and the consideration of crossover transitions allowed to place the other two components of the  $\approx 312$ -keV multiplet within the side band as the  $21/2^+ \rightarrow 19/2^+$  and  $25/2^+ \rightarrow 23/2^+$  transitions. The two transition of 312-keV multiplet included in the  $15/2^+$  band are 310.9- ( $21/2^+ \rightarrow 19/2^+$ ) [0.86 (0.13); -0.09 (0.02)]\* and 312.0-keV ( $25/2^+ \rightarrow 23/2^+$ ) [0.73 (0.13); -0.04 (0.02)]. Their multipolarity values are given in table 6.1, which indicates that these are magnetic dipole transitions.

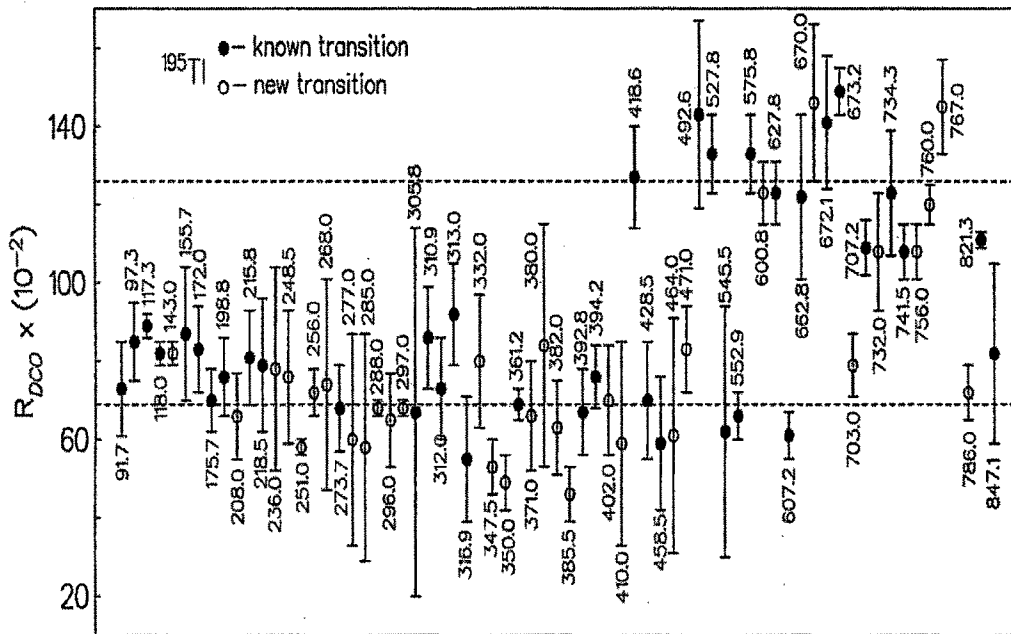


Figure 6.8: Gamma-ray asymmetry  $R_{DCO}$  plotted as a function of the  $\gamma$ -ray energy. The lines have been drawn to guide the eye correspond to the average values of  $\sim 0.69$  for a dipole transition and  $\sim 1.24$  for quadrupole transition when gated on a pure dipole transition. The quoted errors include the errors due to background subtraction, fitting and efficiency correction.

\* Note: the values in the [ ] are DCO, IPDCO ratios respectively.

The other case of doublet occur with  $\approx 673$ -keV observed in the Fig. 6.2. with a greater intensity. When gated on the 310.9- and 312.0-keV transitions we have observed different energies for the 673-keV doublet. These transitions are observed to be 672.1 and 673.2-keV with multipolarities resembling that of an electric quadrupole transitions (ref. Table. 6.1). The experimental coincidence relations can be clearly understood by placing the 672.1- ( $23/2^+ \rightarrow 19/2^+$ ) [1.41 (0.17); 0.09 (0.03)] and 673.2-keV ( $25/2^+ \rightarrow 21/2^+$ ) [1.49 (0.06); 0.17 (0.05)] lines as crossover transitions and in parallel to the 310.9- and 312.0-keV transitions.

In the  $\gamma$ - $\gamma$  coincidence spectra gated on the 458.5- and 175.7-keV lines a  $\approx 117$ -keV peak appears. This line is considered to be a doublet. The two components 117.3- and 118.0-keV, are assigned  $21/2^- \rightarrow 19/2^-$  and  $31/2^+ \rightarrow 29/2^+$  basing on the coincidence data and multipolarity measurements respectively. Their multipolarity values are [0.89 (0.1)] and [0.82 (0.03)] for 117.3- and 118.0-keV respectively.

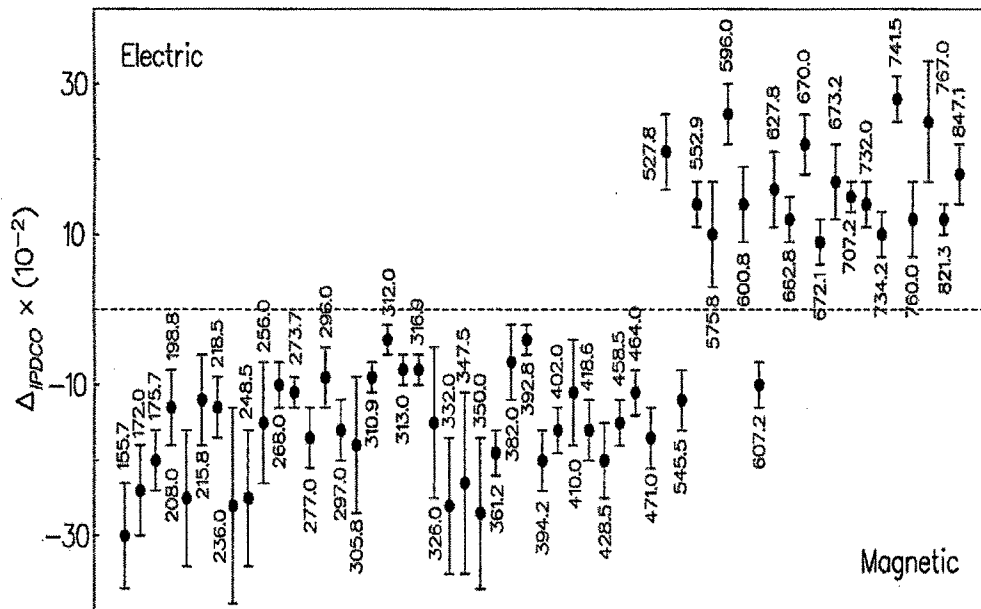


Figure 6.9: Representative experimental  $\gamma$ -ray asymmetry parameter, from polarization measurements plotted for  $\gamma$ -transitions in  $^{195}\text{Tl}$ . A positive value corresponds to an electric transition and a magnetic transition results in a negative value. (Errors as in Fig. 6.6.)

As mentioned earlier the  $\gamma$  transitions found from the present investigation are placed above the  $25/2^-$  level in the  $9/2^-$  band and above the  $25/2^+$  level in the  $15/2^+$  band.

The transition 402-keV has been mentioned in the earlier reported work by Leider *et al.*, [17] but couldn't place it in the level scheme as they were expecting a lower energy  $\gamma$  transitions above the  $25/2^-$  level. We have observed the transition 198.8-keV and which is in coincidence with all the previously known and also the 402-keV transition. Basing on the coincidence measurements and multipolarity arguments this 198.8-keV transition has been placed in the level scheme as  $27/2^- \rightarrow 25/2^-$  [0.76 (0.01); -0.13 (0.05)]. Eventually the 402-keV is placed as  $29/2^- \rightarrow 27/2^-$  [0.70 (0.14); -0.16 (0.03)]. Basing on the similar coincidence relations we have observed 268-, 464-, 296-, 471-, 285-, 382-keV transitions in the  $9/2^-$  band extending the band up to a spin-parity of  $41/2^-$ . These transitions were placed in the level scheme of Fig. 6.1 basing on the coincidence and multipolarity arguments, the values of which are tabulated in table. 6.1. A couple of transitions *viz.*, 309- and 388-keV are also placed in the level scheme but we couldn't assign the multiplicities of these transitions due to lack of enough statistics for these  $\gamma$ -rays.

Apart from these transitions we have observed, their E2 crossover transitions up to spin-parity of  $39/2^-$ . The E2 cross-over transitions are 600.8-, 670-, 732-, 760-, 767-, 756-keV. They are place in accordance with their coincidence and multipolarity measurements. We have observed another band of transitions above the  $29/2^-$  level in the  $9/2^-$  band. These transitions although weak were placed in the level scheme with the help of intensity and multipolarity assignments to many of them (ref. Table. 6.1).

In the earlier paragraphs we have discussed about many doublet and multiplet transitions in this nucleus which made the intensity calculations difficult to perform. In the present investigation we have observed another such doublet at considerably higher spins. The gate on Fig. 6.4 we could observe the transition 296.0-keV. The same transition can be observed in any of the gates in the  $15/2^+$  band (Fig. 6.6, 6.7). This indicates that the transition  $\sim 296$ -keV is in coincidence in both the  $9/2^-$  and  $15/2^+$  bands. This is confirmed with the help of gate on a transition in which the transitions of the other band are not in coincidence. Like when we gate on 458.5-keV (Fig. 6.5) we could observe only the  $\gamma$ -rays in coincidence with the  $9/2^-$  band and in here 296-keV can be clearly observed. And a gate on 175.7-keV (Fig. 6.7) transition can have only the transitions coincidence in  $15/2^+$  band. Here again we can see the 297-keV transition. This establishes that this transition is a doublet transition. Their multiplicities are established and are tabulated in table. 6.1.

The assignment of 607.2- ( $13/2^- \rightarrow 11/2^-$ ) [0.61 (0.06); -0.10 (0.03)] and 552.9-keV ( $15/2^+ \rightarrow 13/2^-$ ) [0.66 (0.06); 0.14 (0.03)] lines within the level scheme of  $^{195}\text{Tl}$  has been placed with the help of multipolarity arguments tabulated in table. 6.1. It is reported in [17] that the transition 418.6-keV ( $15/2^+ \rightarrow 15/2^-$ ) is a pure dipole basing on the angular distribution coefficients. But the present investigation regarding this transition differs from the earlier ones. The 418.6-keV transition has a multipolarity of [1.27 (0.13); -0.16 (0.04)]. This indicates that it is a quadrupole and has magnetic nature. Hence the 418.6-keV  $\gamma$ -ray according to the present calculations is an M2 transition.

Also the transition 847.1-keV decaying to the  $13/2^-$  band from the  $15/2^+$  has a multipolarity of [0.82 (0.23); 0.18 (0.04)]. This indicates that this is an electric dipole transition. It has the initial and final spin-parity of  $15/2^+ \rightarrow 13/2^-$ . The band above  $15/2^+$  has a number of doublets that we have discussed earlier in this chapter *viz.*, 310.9-, 312-keV; 672.1, 673.2-keV. Previously this band has been established up to a spin-parity of  $37/2^+$ . We have added a few more transitions to the existing level scheme with the help of our coincidence and multipolarity calculations. The transitions 297-keV ( $39/2^+ \rightarrow 37/2^+$ ) [0.68 (0.02); -0.16 (0.04)], 350-keV ( $41/2^+ \rightarrow 39/2^+$ ) [0.49 (0.02); -0.27 (0.10)], 410.0 ( $43/2^+ \rightarrow 39/2^+$ ) [0.59 (0.26); -0.11 (0.07)] were well established. The other  $\gamma$ -ray 488.0-keV is found in the coincidence spectra but its multipolarity cannot be assigned unambiguously due to less statistics for the angle dependent gated spectra.

The E2 cross-over transitions in this band can be observed in the  $\gamma$ - $\gamma$  coincidence spectra as seen in Fig. 6.4, 6.6, 6.7. But their spin-parity values cannot be calculated due to less statistics. These nuclei are placed in the level scheme and also in table. 6.1. In the present analysis we could also assign a new band arising from the  $33/2^+$  in the  $15/2^+$  band. This new band above the  $33/2^+$  level consists of all magnetic dipole transitions resembling a magnetic dipole band. These new transitions, level energies, and multipolarity calculations were shown in table. 6.1. Multipolarity calculations can also be observed from the Fig. 6.8. and Fig. 6.9.

**Table 6.1:**  $\gamma$  transition energy ( $E_\gamma$ ) in keV, excitation energy ( $E_x$ ) in keV, DCO ratios ( $R_{DCO}$ ), IPDCO ratios ( $\Delta_{IPDCO}$ ), Multipolarity, initial and final spins for the transitions belonging to  $^{195}\text{Tl}$ .

$E_\gamma$	$E_x$ (Initial Excitaton)	$R_{DCO}^{a,b,c}$	$\Delta_{IPDCO}^c$	$J_i^\pi \rightarrow J_f^\pi$	Multipolarity
91.7	3976.9	0.73 (012)		$31/2^+ \rightarrow 29/2^+$	M1
97.3	2684.3	0.85 (0.1)		$23/2^- \rightarrow 21/2^-$	M1
117.3	2587.0	0.89 (0.03) <sup>b</sup>		$21/2^- \rightarrow 19/2^-$	M1
118.0	4094.9	0.82 (0.03) <sup>b</sup>		$33/2^+ \rightarrow 31/2^+$	M1
143.0	4569.9	0.75 (0.18)		$37/2^+ \rightarrow 35/2^+$	M1
155.7	3885.2	0.87 (0.17)	-0.30 (0.07)	$29/2^+ \rightarrow 27/2^+$	M1
172.0	4266.9	0.83 (0.11)	-0.24 (0.06)	$35/2^+ \rightarrow 33/2^+$	M1
175.7	2212.7	0.70 (0.08)	-0.20 (0.04)	$17/2^+ \rightarrow 15/2^+$	M1
198.8	3156.8	0.76 (0.1)	-0.13 (0.05)	$27/2^- \rightarrow 25/2^-$	M1
208.0	4639.8	0.66 (0.11)	-0.25 (0.09)	$37/2^- \rightarrow 35/2^-$	M1
215.8	3729.5	0.81 (0.12)	-0.12 (0.06)	$27/2^+ \rightarrow 25/2^+$	M1
218.5	4485.4	0.79 (0.17)	-0.13 (0.04)	$37/2^+ \rightarrow 35/2^+$	M1
236.0	4805.9	0.78 (0.26)	-0.26 (0.13)	$39/2^+ \rightarrow 37/2^+$	M1
248.5	3807.3	0.76 (0.17)	-0.25 (0.09)	$31/2^- \rightarrow 29/2^-$	M1
251.0	5056.9	0.58 (0.02) <sup>b</sup>		$41/2^+ \rightarrow 39/2^+$	(M1)
256.0	3412.8	0.72 (0.06)	-0.15 (0.08)	$29/2^- \rightarrow 27/2^-$	M1
268.0	3826.8	0.74 (0.27)	-0.10 (0.03)	$31/2^- \rightarrow 29/2^-$	M1
273.7	2958.0	0.68 (0.11)	-0.11 (0.02)	$25/2^- \rightarrow 23/2^-$	M1
277.0	4431.8	0.60 (0.27)	-0.17 (0.04)	$35/2^- \rightarrow 33/2^-$	M1
285.0	5342.8	0.58 (0.29)		$39/2^- \rightarrow 37/2^-$	M1
288.0	5419.9	0.68 (0.02) <sup>b</sup>		$43/2^+ \rightarrow 41/2^+$	(M1)
296.0	4586.8	0.65 (0.12) <sup>b</sup>	-0.09 (0.04)	$35/2^- \rightarrow 33/2^-$	M1
297.0	4782.4	0.68 (0.02) <sup>b</sup>	-0.16 (0.04)	$39/2^+ \rightarrow 37/2^+$	M1
305.8	1924.2	0.67 (0.47)	-0.18 (0.09)	$17/2^- \rightarrow 15/2^-$	M1
309.0	6034.2				
310.9	2840.5	0.86 (0.13)	-0.09 (0.02)	$21/2^+ \rightarrow 19/2^+$	M1

312.0	3513.7	0.73 (0.13)	-0.04 (0.02)	$25/2^+ \rightarrow 23/2^+$	M1
313.0	1189.9	0.92 (0.13) <sup>b</sup>	-0.08 (0.02)	$13/2^- \rightarrow 11/2^-$	M1
316.9	2529.6	0.55 (0.16)	-0.08 (0.02)	$19/2^+ \rightarrow 17/2^+$	M1
326.0	5131.9		-0.15 (0.10)	$39/2^+ \rightarrow 37/2^+$	M1
332.0	4426.9	0.80 (0.17)	-0.26 (0.09)	$35/2^+ \rightarrow 33/2^+$	M1
347.5	4154.8	0.53 (0.07)	-0.23 (0.12)	$33/2^- \rightarrow 31/2^-$	M1
350.0	5332.4	0.49 (0.0)	-0.27 (0.10)	$41/2^+ \rightarrow 39/2^+$	M1
361.2	3201.7	0.69 (0.04)	-0.19 (0.03)	$23/2^+ \rightarrow 21/2^+$	M1
371.5	3885.2			$29/2^+ \rightarrow 25/2^+$	E2
380.0	5436.9	0.84 (0.31)		$43/2^+ \rightarrow 41/2^+$	(M1)
382.0	5725.2	0.63 (0.12)	0.07 (0.05)	$41/2^- \rightarrow 39/2^-$	M1
385.5	4584.8	0.46 (0.07)		$33/2^- \rightarrow 31/2^-$	(M1)
388.0	6422.2				
390.5	4484.5				
392.8	2011.2	0.67 (0.11)	-0.04 (0.02)	$17/2^- \rightarrow 15/2^-$	M1
394.2	876.9	0.76 (0.08)	-0.20 (0.04)	$11/2^- \rightarrow 9/2^-$	M1
402.0	3558.8	0.70 (0.14)	-0.16 (0.03)	$29/2^- \rightarrow 27/2^-$	M1
410.0	5542.4	0.59 (0.26)	-0.11 (0.07)	$43/2^+ \rightarrow 41/2^+$	M1
418.6	2037.0	1.27 (0.13)	-0.16 (0.04)	$15/2^+ \rightarrow 15/2^-$	M2
428.5	1618.4	0.70 (0.15)	-0.20 (0.05)	$15/2^- \rightarrow 13/2^-$	M1
458.5	2469.7	0.59 (0.17)	-0.15 (0.03)	$19/2^- \rightarrow 17/2^-$	M1
464.0	4290.8	0.61 (0.30)	-0.11 (0.03)	$33/2^- \rightarrow 31/2^-$	M1
471.0	5057.8	0.83 (0.11)	-0.17 (0.04)	$37/2^- \rightarrow 35/2^-$	M1
472.5	3156.8	0.62 (0.07)		$27/2^- \rightarrow 23/2^-$	(E2)
488.0					
492.6	2529.6	1.43 (0.24)		$19/2^+ \rightarrow 15/2^+$	(E2)
515.5	4782.4			$39/2^+ \rightarrow 35/2^+$	E2
527.8	3729.5	1.40 (0.17)	0.21 (0.05)	$27/2^+ \rightarrow 23/2^+$	E2
545.5	2469.7	0.62 (0.32)	-0.12 (0.04)	$19/2^- \rightarrow 17/2^-$	M1
552.9	2037.0	0.66 (0.06) <sup>b</sup>	0.14 (0.03)	$15/2^+ \rightarrow 13/2^-$	E1
575.8	2587.0	1.33 (0.10)	0.10 (0.07)	$21/2^- \rightarrow 17/2^-$	E2

596.0	4154.8		0.26 (0.04)	$33/2^- \rightarrow 29/2^-$	(E2)
600.8	3558.8	1.23 (0.08)	0.14 (0.05)	$29/2^- \rightarrow 25/2^-$	E2
607.2	1484.1	0.61 (0.06) <sup>b</sup>	-0.10 (0.03)	$13/2^- \rightarrow 11/2^-$	M1
624.5	4431.8				
627.8	2840.5	1.19 (0.21)	0.16 (0.05)	$21/2^+ \rightarrow 21/2^+$	E2
647.0	5131.5			$41/2^+ \rightarrow 37/2^+$	E2
662.8	2587.0	1.22 (0.21)	0.12 (0.03)	$21/2^- \rightarrow 17/2^-$	E2
670.0	3826.8	1.46 (0.20)	0.22 (0.04)	$31/2^- \rightarrow 27/2^-$	E2
672.1	3201.7	1.41 (0.17)	0.09 (0.03)	$23/2^+ \rightarrow 19/2^+$	E2
673.2	3513.7	1.49 (0.06)	0.17 (0.05)	$25/2^+ \rightarrow 21/2^+$	E2
703.0	5342.8	0.79 (0.08)		$39/2^- \rightarrow 37/2^-$	(M1)
707.2	1189.9	1.09 (0.07) <sup>b</sup>	0.15 (0.02)	$13/2^- \rightarrow 9/2^-$	E2
732.0	4290.8	1.08 (0.15) <sup>b</sup>	0.14 (0.03)	$33/2^- \rightarrow 29/2^-$	E2
734.3	1924.2	1.23 (0.16) <sup>b</sup>	0.10 (0.04)	$17/2^- \rightarrow 13/2^-$	E2
741.5	1618.4	1.08 (0.28) <sup>b</sup>	0.28 (0.03)	$15/2^- \rightarrow 11/2^-$	E2
756.0	5342.8	1.08 (0.07) <sup>b</sup>		$39/2^- \rightarrow 35/2^-$	(E2)
760.0	4586.8	1.20 (0.05) <sup>b</sup>	0.12 (0.05)	$35/2^- \rightarrow 31/2^-$	E2
767.0	5057.8	1.45 (0.12) <sup>b</sup>	0.25 (0.08)	$37/2^- \rightarrow 33/2^-$	E2
770.0	5409.8				
786.0	4199.3	0.72 (0.07)		$31/2^- \rightarrow 29/2^-$	(M1)
821.3	2011.2	1.11 (0.02)	0.12 (0.02)	$17/2^- \rightarrow 13/2^-$	E2
847.1	2037.0	0.82 (0.23)	0.18 (0.04)	$15/2^+ \rightarrow 13/2^-$	E1
851.3	2469.7				

<sup>a</sup> calculations done with gate on quadrupole transitions; <sup>b</sup> calculations done with gate on dipole transitions; <sup>c</sup> the quoted errors observed in DCO and IPDCO values are due to background subtraction, fitting and efficiency correction

### 6.5. Conclusions

The level scheme of  $^{195}\text{Tl}$  in the vicinity of  $Z \sim 82$  proton shell closure populated through the reaction  $^{181}\text{Ta}(^{18}\text{O}, 4n)^{195}\text{Tl}$  has been deduced. AFRODITE gamma detector array consisting of 8 Compton suppressed Clover detectors and 6 LEPS detectors were used to detect the de-exciting  $\gamma$ -rays. More than 40 new transitions belonging to this nucleus have been identified and placed in the level scheme with the help of coincidence and multipolarity arguments. The existing level scheme and the two bands associated with it were extended to higher spins and excitation energy. As established the band  $9/2^-$  is a result of the coupling of  $h_{9/2}$  proton to the corresponding core nuclei  $^{194,196,198}\text{Hg}$  respectively. And it is assumed that the  $15/2^+$  positive parity band arises from the vector coupling of  $h_{9/2}$  proton aligned along the symmetry axis, and the broken neutron pair consisting of a rotation-aligned  $i_{13/2}$  neutron and a strongly coupled low- $j$  neutron in the  $p_{1/2}$ ,  $p_{3/2}$  or  $f_{5/2}$  shell. Such nuclei have all the important features stated above and there is a need for more theoretical calculations to understand the underlying mechanism in such nuclei.

**References**

1. R.M. Diamond and F.S. Stephens, Nucl. Phys. 45, 632 (1963)
2. J.O. Newton, S.D. Cirilov, F.S. Stephens, and R.M. Diamond, Nucl. Phys. A 148, 593 (1970)
3. J.O. Newton, F.S. Stephens and R.M. Diamond, Nucl. Phys. A 236, 225 (1974)
4. M.G. Slocombe, J.O. Newton and G.D. Dracoulis, (Private Communication)
5. A.C. Kahler, L.L. Riedinger, N.R. Johnson, E. Eichler, P. Hubert, G. J. Smith and R.L. Robinson (Private Communication)
6. D. Venos, J. Adam, J. Jursik, A. Kuklik, L. Maly, A. Spelck, L. Funke and P. Kemnitz, (Private Communication) (1976)
7. D. Proetel, D. Benson, Jr., A. Gizon, M.R. Maier, R.M. Diamond and F.S. Stephens, Nucl. Phys. A 226, 237 (1974)
8. H. Beuscher, W.F. Davidson, R.M. Lieder, A. Neskakis and C. Mayer-Boricke, Phys. Rev. Lett. 32, 843 (1974)
9. J. Meyer-ter-Vehn, F.S. Stephens and R.M. Diamond, Phys. Rev. Lett. 32, 1383 (1974); J. Meyer-ter-Vehn, Nucl. Phys. A 249, 111, 141 (1975)
10. G. Leander, Nucl. Phys. A 273, 286 (1976)
11. H. Toki, (Private Communication)
12. Amita, A.K. Jain, B. Singh, At. Data Nucl. Data Tables 74, 273 (2000)
13. P. Willsau et al., Z. Phys. A 355, 129 (1966)
14. B. Cederwall et al., Phys. Rev. C 47, R2443 (1997)
15. A.N. Wilson et al., Phys. Lett. B. 505, 6 (2001)
16. A.J. Kreiner *et al.*, Phys. Rev. C 20, 2205 (1979)
17. R.M. Leider *et al.*, Nucl. Phys. A 299, 255 (1978)
18. A.J. Kreiner *et al.*, Nucl. Phys. A 308, 147 (1978)
19. B. Singh, R. Zywina, R.B. Firestone, Nucl. Data Sheets 97, 241 (2002)
20. A.J. Kreiner *et al.*, Nucl. Phys. A 282, 243 (1977)
21. A.J. Kreiner *et al.*, Phys. Rev. C 22, 2570 (1980)
22. A.J. Kreiner *et al.*, Phys. Rev. C 23, 748 (1981)
23. D.C. Radford, Nucl. Inst. Meth. A 361, 297 (1995)
24. S.S. Ghugre, S.B. Patel, M. Gupta, R.K. Bhowmik, and J.A. Shiekh, Phys. Rev. C 50, 1346 (1994)

25. F.S. Stephens, M.A. Delenplanque, R.M. Diamond, A.O. Macchiavelli, and J.E. Draper, *Phys. Rev. Lett.* **54**, 2584 (1985)
26. C.W. Beausang *et al.*, *Nucl. Instrum. Methods Phys. Res. A* **364**, 560 (1995)
27. G Duchene *et al.*, *Nucl. Instrum. Methods Phys. Res. A* **432**, 90 (1999)
28. Droste Ch *et al.*, *Nucl. Instrum. Methods Phys. Res. A* **337**, 430 (1999)
29. Starosta K *et al.*, *Nucl. Instrum. Methods Phys. Res. A* **423**, 16 (1999)
30. Krishichayan *et al.*, *Eur. Phys. J. A* **29**, 151 (2006)
31. Krishichayan *Thesis submitted to the University of Calcutta*, (Unpublished) (2007)